Transgenic porcine model reveals two distinct LGR5-positive cell populations during lung development and homeostasis

Kathryn M. Polkoff[1,2], Nithin K. Gupta[2,3], Yanet Murphy[1,2], Ross Lampe[1,2], Jaewook Chung[1,2], Amber Carter[1,2], Jeremy M. Simon[4], Katherine Gleason[1,2], Adele Moatti[2,5], Preetish K. Murthy[6], Laura Edwards[1,2], Alon Greenbaum[2,5], Aleksandra Tata[6], Purushothama Rao Tata[6], Jorge A. Piedrahita*[1,2]

Author Affiliation:

[1] Department of Molecular Biomedical Sciences, College of Veterinary Medicine, North Carolina State University, Raleigh, NC 27607, USA

[2] Comparative Medicine Institute, North Carolina State University, Raleigh, NC 27607, USA

[3] Campbell University School of Osteopathic Medicine, Lillington, NC 27546, USA

[4] Department of Genetics, University of North Carolina School of Medicine

[5] Joint Department of Biomedical Engineering, University of North Carolina at Chapel Hill and North Carolina State University, Raleigh/Chapel Hill, NC 27607/27599, USA

[6] Department of Cell Biology, Duke University School of Medicine, Durham, NC, USA

* Corresponding Author Jorge A. Piedrahita
Department of Molecular Biomedical Sciences and Comparative Medicine Institute
North Carolina State University japiedra@ncsu.edu

ABSTRACT
LGR5 stem cells play a pivotal role in homeostasis, repair, and regeneration in multiple organs including skin and gastrointestinal tract, yet little is known about their role in the lung. Furthermore, findings from mice, a widely used animal model, suggest that LGR5 expression differs drastically from that of humans. In this work, using a new transgenic pig model, we identify two populations of LGR5+ cells in the lung that are conserved in human, but not mouse lungs. Using RNA sequencing, 3D imaging, organoid models, and differentiation assays, we determine that in the fetal lung, epithelial LGR5 expression is transient in a subpopulation of SOX9/SFTPC-expressing lung tip cells. In contrast, epithelial LGR5 expression is absent from postnatal lung, but is reactivated in bronchioalveolar organoids derived from basal airway cells. We also describe a separate population of mesenchymal LGR5$^+$ cells that surrounds developing and mature airways, lies adjacent to airway basal cells, and is closely associated with nerve fibers. Transcriptionally, mesenchymal LGR5+ cells are a subset of peribronchial fibroblasts populations and express unique patterns of WNT and TGF-β signaling pathway genes. These results support two distinct roles for LGR5+ cells in the lung and describe a physiologically relevant animal model for further studies on the function of these populations in repair and regeneration.

Introduction

LGR5 is a known potentiator of WNT signaling (1), is often involved in developmental processes and regeneration, and generally marks key progenitor populations in organ development and postnatal homeostasis. Originally identified in the mouse intestine (2), LGR5$^+$ populations have been identified in a number of mouse tissues and organs (3). In humans, before the advent of scRNA-seq, information of LGR5 cells has been sparse due to lack of reliable antibodies. Overall, the role of LGR5 cells in the lung has been largely unstudied in both mice and humans.

WNT signaling is vital to lung development (4, 5) in addition to repair and regeneration (6). Furthermore, RSPO2, a ligand for LGR5, was shown to have a vital role in lung branching morphogenesis, and the limited lung growth resulting from inactivation of *RSPO2* was correlated with reduced canonical WNT signaling (7). These observations suggest a potential role for LGR5 signaling in lung development. While distribution of lung Lgr5$^+$ cells has not been described in fetal mice, in humans, using scRNA-seq, an *LGR5*$^+$ epithelial population was reported in the elongating bud tip of the fetal lung (8). In the postnatal lung, a study of *Lgr5* expression in mice describes *Lgr5*$^+$ mesenchymal cells which are absent from the airways but centered around the alveolar progenitor cells orchestrating the alveolar niche (9). In humans, using scRNA analysis, *LGR5*$^+$ mesenchymal cells were identified as airway-associated peribronchial fibroblasts (10, 11). Wang et al (12) also reported overexpression of LGR5 in patients with lung adenocarcinoma supporting a role of lung LGR5 cells in both health and disease.

The disconnect between human and murine findings reinforces the need for an animal model that represents a more faithful anatomical and physiological model to the human lung (13–18) and can be used to study the function of lung LGR5 cells. Here we used a validated transgenic porcine model expressing a nuclear-localized histone H2B–GFP under the control of the endogenous *LGR5* promoter (19). This animal model faithfully identifies LGR5+ cells, and we have shown that the H2B-GFP expression correlates spatially and quantitatively with LGR5 mRNA expression by RNA in situ hybridization and quantitative PCR (19). Using this model we show that in pig lungs there are two

populations of LGR5$^+$ cells in homeostasis and development. In the developing lung, epithelial expression of LGR5 is tightly coupled with elongating bud tips and is only present during fetal development. Additionally, in the developing and postnatal lung, LGR5 expression defines a mesenchymal cell surrounding the airways. We also report the unique 3D spatial arrangement of each population, confirm their presence in humans, and examine a potential role for LGR5 in epithelial regeneration. We moreover define the spatial organization and transcriptional signature of the mesenchymal population. This large animal model provides a new avenue for further understanding the role of LGR5 cell populations in lung development, possible contribution to lung diseases such as lung adenocarcinoma, IPF and COPD, and in forging lung repair and regeneration.

Results

Distinct and dynamic expression of LGR5 in developing lung bud tips and peribronchial mesenchymal cells.

To understand the spatial distribution of LGR5 expression throughout development and homeostasis, we used the *LGR5-H2B-GFP* transgenic porcine model (19). Fetal lungs co-stained with EpCAM for epithelial cells and vimentin for mesenchymal cells shows that in the fetal lung two LGR5$^+$ populations exist: one mesenchymal, in the peribronchial area surrounding the airways, and one epithelial, in the bud tips (Figure 1A-C). In the postnatal lung, only the peribronchial LGR5$^+$ mesenchymal population is present, surrounding the airways and occupying a sub-basal position directly adjacent to the airway epithelium (Fig 1D-F). For spatial mapping of the LGR5-expressing cells, we used whole-tissue clearing technique (20) and light sheet microscopy to acquire 3D images of fetal gestational day 80 (GD80) and juvenile porcine lungs (Supplementary Video). In the fetal lungs, mesenchymal LGR5 expression is robust, surrounding both proximal and developing distal airways, but absent in bud tips. Airway epithelial cells in the fetus are LGR5 negative except at the bud tips (Figure 1G). In the postnatal lung, in contrast, the peribronchial mesenchymal population surrounding the airways expresses LGR5, but no LGR5+ epithelial cells are detected (Figure 1H). To determine whether the distribution of LGR5+ cells in the developing and postnatal pig lungs is representative of the human, we employed fluorescent *in situ* hybridization (FISH) to detect *LGR5* mRNA transcripts in human fetal and adult lung tissue. *LGR5* expression is robust in human fetal lung bud tips (Figure 1I), with an almost identical pattern of expression as the pig (as in 1C). In addition, *LGR5* expression was detected in the subepithelial population surrounding maturing airways, as shown with co-staining with SCGB3A2, a marker of developing airway epithelium (Figure 1J). Finally, robust detection of *LGR5* is evident in the peribronchial region of adult airways (Figure 1K). These data support that there are at least two distinct LGR5$^+$ populations in the lung, and that their presence is consistent in humans and pigs, but differs from what has been reported in mice (9).

Transient and conserved expression patterns of LGR5 in human and pig epithelial populations in developing lung bud tips

We next examined the marker expression of the epithelial LGR5$^+$ population at the pseudoglandular gestational day 50 (GD50) and canalicular stage (GD80). We compared expression of LGR5 with markers of bud tips, including SOX9 and SFTPC (21), as well as a marker for more developed airway cells, SOX2 (22). The pattern of LGR5 expression in developing bud tips is stochastic, with LGR5$^+$ cells intercalated within the SOX9 cells throughout the lung bud tips (Figure 2A, 2D and 2I). Quantification of the proportion of LGR5$^+$ epithelial cells that also express SOX2 shows that they are

co-expressed significantly more in the pseudoglandular stage (GD50), than in the canalicular stage (GD80), where there is almost no overlap between LGR5 and SOX2 expression (Figure 2G) ($P<0.05$). In contrast, all LGR5$^+$ epithelial cells express SOX9, at both GD50 and GD80 (Fig 2H) with 42% of SOX9$^+$ bud tip cells also expressing LGR5 at GD50, but by GD80 that number is reduced to 22.2% (Figure 2H)($P<0.05$). Combined, these results suggest that epithelial LGR5 expression is increasingly restricted as the cells transition from SOX9 to SOX2 expression (tip versus stalk). Moreover, *RSPO2*, a known ligand of LGR5, is detectable in the stromal region of the developing bud tip near LGR5 cells at both GD50 (Figure 2J-K) and GD80 (Figure 2L-M). LGR5 expression is also correlated with epithelial SFTPC expression, confirming that the epithelial LGR5 expression is specific to bud tips (Figure 2N-O red arrow), while the mesenchymal population does not express SFTPC (Figure 2O, white arrow).

For an initial high-resolution transcriptome analysis of LGR5$^+$ epithelial cells, we performed a scRNA-seq screen on fluorescence-activated cell sorted (FACS) fetal lung LGR5$^+$ (H2B- GFP positive) cells from GD80, a stage where both mesenchymal and epithelial cell populations coexist. We identified a total of four epithelial (EpCAM+) and ten mesenchymal (VIM+) cell clusters (Figure 3A-3C) and identified genes that can be used to relate each cluster to established human developmental populations. Among the four EpCAM$^+$ cell types, expression patterns of bud tip progenitors (*SFTPC, SFTPB, ETV4* and *ETV5)*, as well as other known markers of bud tip-adjacent stalk region and/or genes known to impact lung development such as *FOXA2, FOXP2* and *NGFR* (Figure 3D), differed. Cluster Epi 4, for instance, likely represents a more differentiated cell type, with increased expression of the basal cell markers *NGFR, KRT5*, and *KRT14*, and reduced expression of lung tip markers *SFTPB, SFTPC* and *ETV5* (Figure 3E). At this point we have not been able to convincingly assign the different mesenchymal subpopulations to specific cell types nor whether they represent a maturing lineage(s). It does show, however, the complexity of the LGR5 mesenchymal population.

Functional analysis of fetal and adult epithelial cells via organoid modeling shows LGR5 expression is reactivated in vitro and is associated with organoid forming efficiency and cell fate

As the expression of LGR5 is increasingly restricted in the epithelial population between GD50 and GD80, we next asked whether LGR5 expression and developmental stage impacted their ability to form organoids. LGR5$^+$ or LGR5$^-$ epithelial cells were sorted from fetal GD50 or GD80 lungs and plated in 3D culture. In the given culture conditions, LGR5$^+$ cells from GD50 organoids formed significantly more organoids than any other group, while there was low organoid formation from GD80 (Figure 4A). Overall, this suggests changes in cell state during development, where the LGR5$^+$ bud tip cells respond differently to inductive signals depending on the stage of development.

In addition, postnatal airway epithelial cells, which do not express LGR5, were seeded under the same conditions as the fetal cells. After 5-7 days in culture, a few organoids displayed visually detectable LGR5$^+$ cells, and by day ten, most, if not all, organoids had LGR5$^+$cells (Figure 4B). We next asked if there were any differences between the behavior of organoid-derived LGR5$^+$ and LGR5$^-$ cells. After dissociation, the LGR5$^+$ and LGR5$^-$ populations were sorted (Figure 4C) and re-seeded in matrigel. We observed no detectable difference between the two populations in organoid forming efficiency, and organoids from the LGR5$^-$ population once again reactivated LGR5 (Figure 4C).

To ask which cells reactivated LGR5 expression and formed organoids, we plated sorted lung cells based on NGFR, a known basal cell marker, and EpCAM (Figure 4D). The EpCAM$^+$/NGFR$^+$ basal cell

population formed significantly more organoids per well at the same concentration than the EpCAM$^+$/NGFR$^-$ cells, but both expressed LGR5 and had mixed LGR5$^+$ and LGR5$^-$ organoids, suggesting that, although NGFR$^+$ basal cells were the primary driver of organoid formation, the basal cells and non-basal cells had similar fate under these conditions.

This observation led us to ask what the cell state of the organoid LGR5$^+$ versus LGR5$^-$ cells is by RNA-seq analysis (Supplement Figure 1). Among the top significantly upregulated genes in the LGR5$^+$ population were *SFTPC, KRT14, AXIN2*, both markers of club/secretory cells or specialized progenitor basal and AT2 cells (23), which are also co- expressed in LGR5$^+$ cells in bud tip development. In addition, LGR5$^+$ cells upregulated *BMP4*, *BMPR1B* and *TGFB2*, all known regulators of lung airway development (24). Among the genes downregulated in LGR5$^+$ cells were *AQP5*, an alveolar AT1 cell marker (25) *LTF*, a marker for differentiating basal cells (11) and *FRZB, FZD6* and *FST*, known negative regulators of canonical WNT signaling (26–28).

Given the shared markers of LGR5$^+$ organoid cells with lung development markers, we hypothesized that the LGR5 expression was related to cell fate. To test this, we altered the media conditions from a bronchioalveolar fate to a bronchiolar phenotype by removing WNT and WNT agonist CHIR. After ten days in culture, none of the bronchiolar organoids expressed LGR5, while the bronchioalveolar were LGR5$^+$ (Figure 4E). To confirm the phenotype of each condition, we examined expression of KRT14 (basal cell marker) and SFTPC (29) (Figure 4F). This suggests LGR5 is only expressed when airway epithelial cells are differentiating toward an alveolar fate, but not when they maintain a basal cell state.

Adult LGR5$^+$ mesenchymal cells form a unique niche in the peribronchial region and express a stromal cell gene signature

As myofibroblasts are a known mesenchymal population surrounding airways, we asked if LGR5$^+$ cells in the adult lung were αSMA$^+$ myofibroblasts. As shown in Figure 5A-F, LGR5$^+$ and αSMA$^+$ populations remain separate; in proximal airways the LGR5$^+$ cells are located between the αSMA cells and the airway epithelial cells (Figure 5B-C), and in the distal bronchioalveolar region the two populations are intercalated surrounding the basal layer (Figure 5E-F), suggesting separate but co-existing roles for αSMA$^+$ and LGR5$^+$ populations. This is further demonstrated by a 3D image of a proximal airway showing how the LGR5 and αSMA are arranged in perpendicular orientation to each other (Figure 5G-H). Furthermore, most of the mesenchymal LGR5$^+$ cells are located directly adjacent to the NGFR$^+$ basal cells, separated by the airway epithelium basal membrane (Figure 5I). We also noted that at GD80, a stage that encompasses well developed to inmature airways, the distribution of the LGR5$^+$ cells differed between proximal and distal airways with the degree of spatial organization both longitudinally and circumferentially decreasing proximally to distally (Figure 5J-L).

As the LGR5$^+$ cells occupy a niche directly adjacent to the airway basal cells, and since the LGR5 receptor is a potentiator of WNT signaling, we asked which WNT family genes were significantly enriched in the LGR5$^+$ population by comparing the transcriptome of LGR5$^+$ and LGR5$^-$ postnatal mesenchymal cells (Figure 5M-N). LGR5$^+$ cells express canonical and non-canonical WNT signals, such as *WNT5A, RYK, ROR1, ROR2, and GPC4*, in addition to known negative regulators of WNT signaling, such as SFRP1, *SFRP2 and PRICKLE2*. Furthermore, they upregulate WNT self-responsive signals such as *FZD1, FZD2* and *AXIN2* (Figure 5M)(30). We also examined TGF-β pathway genes as they are known to be involved in lung development and disease (31–33) and interact with the WNT

pathway (34, 35). As shown in Figure 5N, *TGFB2, TGFB3, BMP4*, *BMP5* and *BMP7* were all upregulated in LGR5$^+$ cells .

To further characterize the LGR5$^+$ cells we applied Gene Set Enrichment Analysis (GSEA) (36) to the top 500 upregulated genes in LGR5$^+$ PD29-38 mesenchymal cells (Supplement Table 1) and examined predicted cell type (Module C8), Gene Ontology:Biological Process, and Gene Ontology:Molecular function. As shown in Supplement Table 2A, the LGR5$^+$ cells have a gene signature that significantly matches adult and fetal stromal cells from multiple organs. Additionally, in spite of being an adult cell, the LGR5$^+$ transcriptional signature not only mapped to fetal cells, but also to GO-Biological Processes related to developmental events including tube development, tube morphogenesis, organ morphogenesis and neurogenesis (Supplement Table 2B). In terms of molecular function, LGR5$^+$ cells are enriched for extracellular matrix constituents and a broad range of binding activity to glycosaminoglycans, heparin, sulfur compounds, collagen, growth factor, calcium and integrin, among others (Supplement Table 2C).

Adult lung mesenchymal LGR5+ cells have multilineage differentiation potential and serve as a signaling niche for airway basal cells

Since the postnatal LGR5$^+$ lung population shared a gene signature with stromal cell and mesenchymal stem cells (Supplement Table 2A), we asked whether the LGR5$^+$ cells were capable of multilineage differentiation. When cultured *in vitro,* LGR5$^+$ cells could differentiate into osteocytes, adipocytes, and chondrocytes (Figure 6A-D). Because stromal cells generally define a support niche for other stem cell subsets, we hypothesized that the LGR5$^+$ cells designate the support niche for airway epithelium. To test this, we isolated NGFR$^+$ basal cells from lung airways and co-cultured at a 1:1 ratio with LGR5$^+$ mesenchymal cells in a matrigel dome with or without growth factors and show that LGR5$^+$ cells alone could support organoid formation from basal cells without additional growth factors (Figure 6E). Furthermore, we noticed that organoids in the LGR5$^+$ co-culture wells, and growth factor only wells, differed morphologically and resembled bronchiolar and bronchioalveolar organoids described in Figure 4F. Quantification of organoid type as previously described (29) shows that the presence of the growth factors induced a bronchioalveolar fate, but LGR5$^+$ mesenchymal stem cells in basic media supported the growth of bronchiolar organoids, and more specifically KRT14$^+$ basal cells (Figure 6F-G).

LGR5 peribronchial mesenchymal cells are associated with nerve fibers and share markers of nerve associated fibroblasts

Based on results of the RNA-seq analysis showing significant enrichment of LGR5$^+$ mesenchymal cells for GO biological processes associated with neuronal development (Supplement Table 2B), the known presence of nerve fibers in proximity to the airways, and the liner-like spatial organization of the cells around the airways, we examined the relationship between LGR5$^+$ cells and expression of PGP9.5, a pan-neuronal marker that has been shown to label nerve fibers in both adult and fetal lungs of multiple species including mice, pigs and humans (37–40) TUJ1, a neuron specific class III beta-tubulin, NGFR/P75 NTR and TRPV1 expressed in sensory C-fibers (41–44) and S100B, a pan-astrocyte markers expressed in glial cell precursors (45, 46). We show that peribronchial LGR5$^+$ mesenchymal cells surrounding the airways express S100B and are organized around nerve fibers that co-express

TUJ1, NGFR/P75 NTR, TRPV1 and PGP9.5 (Figure 7A-W). In contrast, the innervations to the adjacent vessel are devoid of LGR5$^+$ cells (Figure 7X-7Z).

Due to its co-localization with the nerve fibers, as well as expression of S100B, we hypothesized that the LGR5$^+$ cells would share gene signatures with nerve associated fibroblasts or Schwann cells (47). To test this, we examined lung, sciatic and peripheral nerve scRNA-seq datasets from both mouse and human, as well as previously reported canonical markers of nerve associated cells (10, 11, 47–53). Using these data, we compiled a set of markers defining the different nerve fiber-associated and Schwann cell types (Supplement Table 3) and show that LGR5$^+$ cells are highly enriched for markers associated with perineural, epineural and endoneurial fibroblasts but not Schwann cells (Supplement Figure 3). These gene signatures, as well as the spatial colocalization, suggest that the LGR5$^+$ mesenchymal cells may be specialized nerve-associated fibroblasts of as yet unknown function.

Discussion

Here, we show that the pig is an appropriate model for elucidating the role LGR5$^+$ cells in the lung throughout development and homeostasis. While the two described cell populations are consistent in humans (8, 10, 11, 54) and pigs, it is unclear why the results are not consistent with mice. Lgr5 is reported in alveolar fibroblasts in mice, and the roles of the murine Lgr6$^+$ cells seem to be more akin to the LGR5$^+$ human and pig populations (9), given that they surround and support the airway niche. However, the murine Lgr6$^+$ population overlaps significantly with the αSMA$^+$ population in the mouse, whereas the two populations are mutually exclusive in the pig.

We also show that LGR5 expression is heterogeneous in bud tip cells in areas of high RSPO2 expression. That, combined with their position in the fetal airway bud tips, and previous reports that LGR5 itself in the intestinal crypts is correlated with anchoring in a niche (55), suggests that LGR5 may be important for directing tube elongation, controlling lung airway growth, and maintaining an undifferentiated state as the bud tips elongate throughout development. In the adult, epithelial LGR5 expression is absent, yet it's reactivated during bronchioalveolar organoid formation suggesting that this transient pathway may be reactivated during regeneration.

In the mesenchymal population, we identify a peribronchial specific fibroblast population separate from myofibroblasts that is present at homeostasis and suggest a dual role as a mesenchymal stromal cell and a support niche cell for basal cells, and a nerve associated fibroblast involved in communication between the airway cells and the peripheral nervous system. Our RNA-seq data from LGR5$^+$ mesenchymal stem cells show that they secrete canonical WNT inhibitors and upregulate WNT receptors and downstream WNT pathways. Their unique position surrounding the basal cells suggest that the LGR5$^+$ mesenchymal cell may play an active role in blocking ambient WNT signaling from lung interstitium from reaching the airway. Recent work shows that canonical WNT inhibitors promote basal cell stemness (56), while increased canonical WNT signaling promotes basal cell proliferation in airway repair (57). This suggests that LGR5$^+$ cells may influence airway basal cell homeostasis and proliferation by titration of WNT signaling.

More work is needed to determine the role of the LGR5$^+$ mesenchymal cells and the relevance of their close association with the nerve fibers. There are reports of innervation impacting airway branching during development (58), epithelial organ regeneration (59) and being involved in diseases such as asthma and cystic fibrosis (42, 60), yet there is little known what role, if any, LGR5 cells play in these

responses. Studies have also shown activation of a transcriptional injury signature in lung nerves after lung damage (61), which could impact their signaling with the LGR5$^+$ cells in injury. Similarly, abnormal WNT signaling has been reported in COPD, IPF and asthma associated inflammation, airway remodeling and airway hyperresponsiveness (62–64). And while the LGR5+ mesenchymal cells have a signature similar to nerve associated fibroblasts, they appear to be a unique population that is colocalized with lung airway innervation, but not with the innervation of the adjacent blood vessels, suggesting that they are a specialized sub-type of nerve-associated fibroblasts, of as yet unknown function.

The ability to enrich for LGR5$^+$ cells by flow sorting also allows, for the first time, a detailed analysis of these low abundance cells during development, after injury and during disease states. Overall, this new animal model will greatly assist towards the understanding of the role of LGR5 cells during lung development, as well as in the healthy, diseased, and injured lung.

Methods

Transgenic porcine and human tissue

All experiments were carried out in strict accordance with the Institutional Animal Care and Use Committee of North Carolina State University (IACUC protocol 17-028-B), and followed the established ARRIVE guidelines (62). LGR5-H2B-GFP transgenic pigs were generated by somatic cell nuclear transfer as previously described (63). Male and female transgenic offspring were used in these experiments, with no detectable differences. Experiments in this study are performed using lung tissue from 14 postnatal pigs, five fetal GD80 fetuses, five fetal GD50 fetuses. Data are representative of both sexes. Human lung tissues were acquired from sub-transplant-quality lungs from donors without pre-existing lung disease and obtained from the Marisco Lung Institute at the University of North Carolina at Chapel Hill (IRB 03-1396). De-identified human fetal lung tissue sections were obtained from Duke Biorepository & Precision Pathology Center (BRPC). All research using this human fetal lung tissue was approved by the Duke University Institutional Review Board.

Tissue Clearing

We used the BoneClear procedure for clearing the porcine lungs with some adjustments; perfusion, decalcification, and agarose embedding steps were not conducted, and immunostaining occurred over 7 days with anti-GFP primary antibody (Aves Labs, GFP-1010), and Cy3 donkey anti-Chicken IgG (Jackson ImmunoResearch Labs, 703165155). We used a custom light-sheet microscope (64) to image the cleared lungs. The working distance of the detection objective and the field of view was 8 mm and 1.77 mm^2, respectively.

Immunofluorescence

Lung tissue was fixed in 4% paraformaldehyde at 4°C overnight and dehydrated in 30% sucrose before being embedded in OCT. Organoids were fixed in 2-4% paraformaldehyde and embedded in OCT or stained and imaged as whole mounts. Tissues were sectioned using a cryostat set to 20 μM. For immunofluorescent analysis, sections were blocked with 0.4% Triton X-100 and IHC/ICC blocking buffer (Invitrogen) followed by incubation of primary antibody for 1.5 hours at room temperature or 4°C overnight. Primary antibodies were applied at a 1:200 ratio; anti-KI67 (Invitrogen, MA5-14520), anti-EpCAM (Abcam, ab71916), anti-SOX9 (eBioscience, 14-9765-82), anti-SOX2 (Abcam, ab97959), anti-Alpha-Smooth Muscle Actin (Invitrogen 14-9760-82), anti-Vimentin (Santa Cruz, sc-6260),

anti-PDGFRa (Bioss, BSM- 52829R), anti-Prosurfactant Protein C (Abcam, ab90716), SCBG3A2 (Abcam, ab181853). Sections were incubated with secondary antibodies Alexa Fluor 594 Goat Anti-Rabbit (Invitrogen, A-11012) and Alexa Fluor 647 Goat Anti-Mouse (Invitrogen, A-21236) at a 1:500 ratio for 1 hour at room temperature and mounted with Prolong Diamond Antifade Mount with DAPI. Slides were imaged with an Olympus Fluoview 3000 upright confocal microscope.

RNAscope *in situ* hybridization

RNAscope was performed according to the manufacturer's instructions (ACD Bio). Briefly, paraffin embedded lung tissue from human fetus or adult was sectioned at 7 μM. Slides were deparaffinized with xylene, then heat treated followed by protease digestion. The tissue was hybridized with custom probes targeting Hs-SCGB3A2 (544951) and Hs-LGR5 (311021-C2). A positive control probe against human (139-989 region) cyclophilin B or as a negative control, a probe targeting the bacterial gene dapB were tested.

Cell Isolation and Sorting

2-3 cm^2 pieces of lung were collected in cold PBS and minced. Minced tissues were digested at 37°C in an enzymatic digest buffer containing 5 mg/mL Dispase (Invitrogen), 2 mg/mL DNase I (STEMCELL Technologies), and 5 mg/mL (adult) or 2mg/mL (fetal) Collagenase Type II (Sigma). The digestion mixture was strained (70 μM), washed and centrifuged. Pellets were incubated in Red Blood Cell Lysis Buffer (Invitrogen) for 10 minutes at room temperature with gentle agitation. For cell sorting, cells were suspended in MACS buffer (Miltenyi) and incubated with 10μl/ml anti-EpCAM-APC (Thermo Scientific, 17-5791-83) and/or anti-NGFR-PE (eBioscience, 12-9400-41). Propidium iodide was added for dead cell exclusion (Beckman Coulter MoFlo XPD).

Organoid Culture

For generation of lung organoids, 2 x 10^3 cells/droplet were mixed with 25 μl of Matrigel and allowed to solidify upside down at 37°C for 20 minutes and then were overlaid with culture media, which was replaced every other day. Basic growth media consisted of DMEM/F12 (Life Technologies, 12634-010), Glutamax (Life Technologies, 35050-061), HEPES (Life Technologies, 15630-106), N-2 (Life Technologies, 17502-048), B27 (Life Technologies, 12587-010), and 1% antibiotic- antimycotic (Gibco, 15240-096). Bronchioalveolar conditions consisted of LWRN-conditioned media (collected from ATCC CRL-3276) mixed with basic media at a 1:1 ratio, and a growth factor master mix was added for final concentrations of CHIR99021 (PeproTech, 2520691) (5 μM), EGF (PeproTech, AF-100-15) (100 ng/ mL), Nicotinamide (Life Technologies, 17502-048) (2mM), LY2157299 (Cayman Chemical Company 15312) (1 μM), A-83-01 (2 nM), Y27632 (20uM), and FGF10 (16.6ng/mL). For bronchiolar conditions, no LWRN was added and the mastermix contained added R-Spondin (R&D Systems 4645RS/CF) (2 μg/mL), reduced CHIR99021(1 μM), EGF (100 ng/ mL), (Nicotinamide (2mM), LY2157299(1 μM), A-83-01 (2 nM), Y27632 (20 μM), and FGF10 (16.6 ng/mL). For co-culture conditions, $LGR5^+$ mesenchymal cells were mixed at a 1:1 ratio with $NGFR^+$ airway cells (2,000 cells each) and resuspended in a 25 μL droplet of reduced growth factor Matrigel (Corning) overlaid with basic growth media. To dissociate organoids for passage or FACS, ice cold Matrigel Recovery Solution was used.

RNA sequencing analysis

For bulk RNA-sequencing of the adult PD29-38 samples, each group of sorted mesenchymal cells was used for Ultra-low input RNA-seq. Library Preparation, and HiSeq Sequencing RNA library preparations and sequencing reactions were conducted at GENEWIZ, LLC. (South Plainfield, NJ,

USA). For fetal samples, SMART-Seq v4 Ultra Low Input Kit for Sequencing was used for full-length cDNA synthesis and amplification (Clontech, Mountain View, CA), and Illumina Nextera XT library was used for sequencing library preparation. The final library was assessed with Agilent TapeStation. The sequencing libraries were multiplexed and clustered on a flow cell. After clustering, the flowcell was loaded on the Illumina HiSeq instrument according to the manufacturer's instructions. Samples were sequenced using a 2x150 Paired End (PE) configuration. Image analysis and base calling were conducted by the HiSeq Control Software (HCS). Raw sequence data (.bcl files) generated from Illumina HiSeq was converted into fastq files and de-multiplexed using Illumina's bcl2fastq 2.17 software. Sequence reads were trimmed using Trimmomatic v.0.36. The trimmed reads were mapped to the Sus scrofa reference genome available on ENSEMBL using the STAR aligner v.2.5.2b. Unique gene hit counts were calculated by using feature Counts from the Subread package v.1.5.2. Only unique reads that fell within exon regions were counted. After extraction of gene hit counts, the gene hit counts table was used for downstream differential expression analysis. Using DESeq2 (v1.37.6), a comparison of gene expression between the groups of samples was performed. The Wald test was used to generate p-values and Log2 fold changes. Genes with adjusted p-values < 0.05 and absolute log2 fold changes > 1 were called as differentially expressed genes for each comparison. Gene set enrichment analysis was performed using GSEA (Broad Institute) (65, 66) and ClusterProfiler (67).

Single cell RNA sequencing and computational analysis

Single cell suspensions from GD80 fetuses were loaded into a Chromium Controller (10x Genomics) for gel beads in emulsion. After scRNA-seq library preparation with the Chromium SIngle Cell 3' Library & Gel Bead Kit, quality analysis was performed using a bioanalyzer. Libraries were sequenced using an Illumina NextSeq500 system (~400M repair pairs). Barcodes were deconvoluted into a cells x genes matrix using alevin v1.5.2 based on the Sus scrofa Ensembl v11.1.105 assembly, and these counts were imported into R (v4.2.0) for analysis with the Seurat package (v4.1.1) using the RStudio IDE (v2022.07.1). Cells with fewer than less than 5% ribosomal reads and 2000 detected genes were discarded. Unsupervised clustering of the cells was performed with Louvain-Jaccard clustering with multilevel refinement (algorithm=2) implemented in the FindClusters function in Seurat with a resolution of 0.75. Visualizations were generated using the FeaturePlot function in Seurat with Uniform Manifold Approximation and Projection (UMAP) dimensional reduction. The Seurat FindAllMarkers function and Presto (v1.0.0) were used to identify marker genes of each cluster.

Quantification of SOX2/SOX9

Quantification of $SOX2^+$, $SOX9^+$, and $LGR5^+$ cells was performed using ImageJ (NIH). Only epithelial cells were included in the calculations. For SOX2 and LGR5 co-expression, the number of nuclei that expressed both were calculated as a proportion of total $LGR5^+$ cell nuclei. For SOX9 and LGR5 co-expression, it was a proportion of co-expressing nuclei out of the total $SOX9^+$ cells. Statistical analysis comparing ratios of co-expressing cells between D50 and D80 sections was performed using a Welch Two Sample T-test in R, n=10 photos per group, representative of 2 different fetal lungs each.

Mesenchymal stem cell differentiation assay

For adipogenesis and osteogenesis differentiation assays, $LGR5^+$, porcine bone marrow derived mesenchymal stem cells (BMSC) (positive control), and dermal fibroblasts (negative control) were seeded at a density of 50×10^3 cells in 12-well plates and cultured until confluent in a growth medium of DMEM (Corning 10-014-CV), 10% FCS, 1% Antibiotic Antimycotic (Corning 30-004- CI). Differentiation conditions were performed as previously described (68–70). After 4 to 6 weeks for each

condition, cells were fixed and OilRedO, Alizarin Red S, and Alcian Blue applied to detect adipogenic, osteogenic, and chondrogenic differentiation, respectively, and imaged on a Leica Compound Microscope.

Data availability

scRNA-seq data and Seurat objects generated in this study are available from the Gene Expression Omnibus (GEO) under accession code GSE218658. The code to process, analyze and visualize the sequencing data is available at https://github.com/RossLampe/Two_roles_of_LGR5_in_the_lung.

Author Contributions

KMP, NKG, JAP Conceived and designed the analysis
YM, RL, JC, AC, LE, KG Collected the data
AM, AG, JMS, PKM, AT, PRT Contributed data or analysis tools
KMP, YM, RL, JMS Performed the analysis
KMP, NKG, RL, JAP Wrote the paper.

Declaration of Interest

The authors declare no competing interests.

Acknowledgments

This work was supported by awards F31AR077423 to KMP, T34GM131947 to AC, and R21OD019738 to JAP. Authors are grateful to staff at the Laboratory Animal Resources and the Central Procedures laboratories at the College of Veterinary Medicine, North Carolina State University. The single-cell RNA-seq project was facilitated by the Advanced Analytics Core (partially supported by garnet P30 DK034987) and by the Bioinformatics and Analytics Research Collaborative (BARC) at the University of North Carolina at Chapel Hill School of Medicine.

Figure 1. Two populations of LGR5-expressing cells in development and homeostasis in pigs and human lung. (A-C) In the GD80 lung, co-localization with EpCAM (red) or Vimentin (purple) shows that the population surrounding the airways is mesenchymal and surrounds developing large, mid and distal airways, while LGR5$^+$cells in the bud tips are EpCAM$^+$ epithelial cells. (D-F) In the postnatal pig lung, the Vimentin$^+$ mesenchymal population is present in airways of all sizes, and occupies the sub-basal space, but there is no LGR5 expression in epithelial cells. (G) 3D light-sheet microscopy of pig GD80 fetal lung showing LGR5$^+$ cells are an abundant population in the lung and surround the airways as well as being present in the developing bud tips. (H) In the postnatal lung, LGR5 is expressed only surrounding the airways. (I-K) Conservation of *LGR5* populations between humans and pigs. *In situ* hybridization with a probe detecting human *LGR5* transcripts in human developing lung shows the presence of epithelial *LGR5* expression in gestational day 135 bud tips (white arrows) (I), and the presence of the mesenchymal *LGR5* expression in cells directly adjacent to the airway epithelium (stained with SCGB3A2) in both fetal day 142 (J) and adult (K) airways. Scale bars are equivalent to 100 μM.

Figure 2. Epithelial LGR5$^+$ cells are spatially located in the distal portion of elongating lung bud and become more distally restricted as development progresses. (A-F) Representative images of the relationship between LGR5 and SOX9, a known marker of developing bud tips, and SOX2, a marker of more differentiated airways. (G) Quantification of LGR5 and SOX2 co-expression, represented as percentage of co-expressing cells over total LGR5$^+$ cells. co-expression is significantly reduced between GD50 and GD80 ($p<0.0005$, Welch two sample t-test, n=10 images representative of sections from 2 different fetal lungs each). H) Percentage of LGR5$^+$/SOX9$^+$ as a proportion of total SOX9$^+$ cells decreases from GD50 to GD80 ($p<0.05$, Welch two sample t-test n=10 images, 2 different fetal lungs each). (I) 3D visualization of LGR5 and SOX9 expression at GD80 via whole-mount confocal imaging showing intercalated SOX9 and LGR5 expression in lung bud tips. (J-M) Expression of RSPO2 in the region surrounding bud tips. (N) GD50 fetal lung showing co-expression (red arrow) of LGR5 and the known lung bud tip marker SFTPC. (O) GD80 fetal lung showing co-expression of LGR5 and SFTPC in the lung bud epithelial cell (red arrow) but not the LGR5$^+$ mesenchymal cells surrounding the airways (white arrow).

Figure 3. Single cell RNA sequencing of GF80 fetal porcine LGR5$^+$ cells confirm the presence of epithelial and mesenchymal LGR5$^+$ populations during development. All LGR5$^+$ cells were FACS sorted from porcine fetal GD80 lung, and after quality assessment and filtering, 5,284 cells were retained for analysis. A) UMAP analysis identified two main populations marked by differential expression of EpCAM and Vimentin. (B-C) Presto marker analysis identified nine mesenchymal clusters and four epithelial sub-clusters. (D) Examination of LGR5 expression in all clusters showed that mesenchymal populations 1-7 had higher levels of LGR5 expression than the remaining mesenchymal populations or the epithelial populations. (E) In addition, the four epithelial subclusters expressed differing levels of multiple lung bud tip markers such as SFTTPC, KRT14 and SOX9 as well as RSPO2 and RSPO3 (Epi 1).

Figure 4. **LGR5 expression is transiently reactivated in adult epithelial organoids and is associated with organoid forming efficiency and cell fate.** (A) Organoid formation efficiency of EPCAM$^+$/LGR5$^+$ or EPCAM$^+$/LGR5$^-$ cells from GD50 or GD80 fetal pigs with GD50 EPCAM$^+$/LGR5$^+$ cells demonstrating the highest formation efficiency. Comparison of all pairs was performed using a one-way ANOVA by group, and comparison of means was performed by Tukey-Kramer HSD, n=3 biological and 10 technical replicates for each group, $p<0.05$ (B) EPCAM$^+$/LGR5$^-$ cells from adult lungs were placed in organoid culture. While organoids remained LGR5$^-$ after 4 days of culture, by 5-7 days LGR5 expression was detectable. By day 10, a mixture of LGR5$^+$ and LGR5$^-$ organoid could be detected. Scale bars represent 300 uM. (C) After 10 days in culture, organoids were dissociated and sorted by EPCAM and LGR5 expression. EpCA EPCAM$^+$/LGR5$^-$ and EPCAM$^+$/LGR5$^+$ cells were plated separately for organoid formation, and both populations generated a mixture of LGR5 positive and negative organoids. Scale bar represents 300 uM. (D) LGR5 adult lung cells were sorted based on expression of EpCAM and NGFR (an airway basal cell marker) and EpCAM$^+$/NGFR$^+$ and EpCAM$^+$/NGFR$^-$ cells were plated separately for organoid formation efficiency. EpCAM$^+$/NGFR$^+$ epithelial cells formed organoids at a significantly higher efficiency than EpCAM$^+$/NGFR$^-$ cells ($p<0.001$, Welch two sample t-test, n=3 biological and 4 technical replicates each). (E) Postnatal epithelial cells (LGR5$^-$) were cultured in bronchioalveolar or bronchiolar organoid media and imaged by fluorescent or brightfield microscopy. Only bronchioalveolar culture conditions induced LGR5 expression. Scale bar represents 300 uM (F) Organoid type (bronchiolar versus bronchioalveolar) was confirmed by

morphology and by IHC using antibodies to SFTPC and KRT14. Scale bars represent 900 uM.

Figure 5. LGR5$^+$ mesenchymal populations are distinct from myofibroblasts, have a highly organized spatial distribution in the mature airways, lie in proximity to airway basal cells and have a unique transcriptional profile. (A-F) Confocal imaging of bronchiolar (A-C) and bronchioalveolar (D-F) cross-sections, shows that LGR5$^+$ cells are distinct from αSMA expressing smooth muscle and myofibroblasts. In the mature airways LGR5$^+$ cells are located between the αSMA$^+$ layer and the lung airway epithelial cells, and in the distal airways/bronchioalveolar region, LGR5$^+$ and αSMA$^+$ are separate, but closely positioned surrounding the airways. (G-H) 3D rendering of whole mount tissue shows the longitudinal arrangement of the LGR5+ cells perpendicular to the orientation of the αSMA$^+$ cells. (I) Close apposition between LGR5$^+$ cells and the basal airway epithelial cell identified by NGFR. (J-L) Spatial organization in GD80 whole mount confocal images, with both longitudinal and circumferential alignment in large proximal airways (I), primarily longitudinal alignment in smaller airways (J), and more random organization in distal airways near the elongating bud tips (K). Scale bar indicates 100 μM unless marked otherwise. (M) KEGG WNT and (N) KEGG TGF-β pathways genes upregulated in postnatal (PD29-PD38) LGR5$^+$ mesenchymal cells.

Figure 6. Postnatal LGR5$^+$ cells are mesenchymal stromal cells and support the airway basal cell niche. (A) LGR5$^+$ mesenchymal cells were cultured in osteocyte, adipocyte or chondrocyte differentiation media to examine whether they had multilineage properties. (B-D) LGR5$^+$ cells show the ability to differentiate into osteocytes (B), adipocytes (C), and chondrocytes (D). Porcine bone marrow mesenchymal stem cells were used as a positive control, and porcine dermal fibroblasts as negative controls. (E) Airway basal cells were seeded in growth factor deficient Matrigel either with no additional factors, in a 1:1 ratio with LGR5$^+$ mesenchymal cells only, or with 1:1 ratio of LGR5$^+$ mesenchymal cells and a growth factor cocktail. (F) Bronchiolar organoids were characterized by a spherical shape, robust expression of KRT14, and absence of SFTPC. Bronchioalveolar organoids had an irregular shape and expressed both SFTPC and KRT14. Representative images are shown. G) Proportion of organoid type for each growth condition. Organoids from epithelial cells co-cultured with LGR5$^+$ cells only were primarily bronchiolar, while conditions containing LGR5$^+$ cells and growth factors or growth factors alone yielded primarily bronchioalveolar organoids. *** indicates $p<0.005$, ANOVA for each treatment followed by pairwise t-tests to determine significant differences, points represent n=3 biological replicates which each included at least 25 organoids per group.

Figure 7. LGR5$^+$ mesenchymal cells orient themselves along peripheral nerve fibers and express markers of nerve-associated fibroblasts. LGR5$^+$ cells identified by their intense nuclear GFP orient themselves along PGP 9.5 positive fibers and express S100B at fetal GD80 (A-G) and adult PD29-38 (H-N). LGR5 nuclei align in an organized pattern with the longitudinal neuronal fibers of the airways. (A-B) Sagittal section showing rows of LGR5 cells running longitudinally and corresponding to the location of PGP 9.5 fibers (white arrow) (C) Cross-section of airway showing the localization of the PGP 9.5 fibers below the airway (AW) basal membrane (white arrow). (D and K) Higher magnification of a sagittal section shows that this co-localization also occurs in lateral fibers (white arrow). The punctate red staining represents cross-sections of nerve fibers, many of them in direct contact with the LGR5 cell near the nuclear region (yellow arrows). Note that while the LGR5 cells are in contact with PGP 9.5 -expressing fibers, they themselves are PGP 9.5 negative. (E-G and L-N) staining with S100B, a known Schwann cell lineage maker, showing that many, if not all fetal and postnatal LGR5 cells, also stain for S100B. (G) LGR5$^+$/S100B$^+$ cells co-localize to ganglions with concentrations of neuronal cell bodies

(white arrow). (O-W) Co-localization with LGR5$^+$ cells with TUJI positive (O-Q), NGFR (R-T) and TRPV1 (U-W) in postnatal nerve fibers. (X-Z) Cross-section of postnatal airways showing presence of LGR5$^+$ cells in the innervation surrounding the airways but not the blood vessels (BV). Scale bars are equivalent to 100 μM.

Supplementary Information

Supplement Figure 1. Volcano plot of differentially expressed bud tip markers and WNT and TGF-beta pathway genes of LGR5+ versus LGR5$^-$ organoid-derived epithelial cells.

Supplement Figure 2. Volcano plot for differentially expressed genes in LGR5$^+$ versus LGR5$^-$ lung mesenchymal cells that are known markers of nerve-associated fibroblasts (Perineurial, epineurial, and endoneurial), or Schwann cells (Schawnn cells, non-myelinating SC, and myelinating SC).

Supplement Table 1. Top 500 Upregulated genes in postnatal (PD29-38) LGR5+ mesenchymal cells**.**

Supplement Table 2. Gene Set Enrichment Analysis for cell type (Module C8), Gene Ontology:Biological Process, and Gene Ontology:Molecular function using the top 500 upregulated genes in LGR5$^+$ PD29-38 mesenchymal cells.

Supplement Table 3. Summary of markers of nerve-associated cells and Schwann cells used to generate Supplement Figure 2.

Supplement Video 1. Fetal and adult lung light-sheet microscopy. Associated with images in Figure 1.

REFERENCES

1. Barker N, Tan S, Clevers H. Lgr proteins in epithelial stem cell biology. *Development* 2013;140:2484–2494.
2. Barker N, van Es JH, Kuipers J, Kujala P, van den Born M, Cozijnsen M, *et al.* Identification of stem cells in small intestine and colon by marker gene Lgr5. *Nature* 2007;449:1003–1007.
3. Leung C, Tan SH, Barker N. Recent Advances in Lgr5+ Stem Cell Research. *Trends Cell Biol* 2018;28:380–391.
4. Kadzik RS, Cohen ED, Morley MP, Stewart KM, Lu MM, Morrisey EE. Wnt ligand/Frizzled 2 receptor signaling regulates tube shape and branch-point formation in the lung through control of epithelial cell shape. *Proc Natl Acad Sci U S A* 2014;111:12444–12449.
5. Hussain M, Xu C, Lu M, Wu X, Tang L, Wu X. Wnt/β-catenin signaling links embryonic lung development and asthmatic airway remodeling. *Biochim Biophys Acta Mol Basis Dis*

2017;1863:3226–3242.

6. Raslan AA, Yoon JK. WNT Signaling in Lung Repair and Regeneration. *Mol Cells* 2020;43:774–783.
7. Bell SM, Schreiner CM, Wert SE, Mucenski ML, Scott WJ, Whitsett JA. R-spondin 2 is required for normal laryngeal-tracheal, lung and limb morphogenesis. *Development* 2008;135:1049–1058.
8. Hein RFC, Wu JH, Holloway EM, Frum T, Conchola AS, Tsai Y-H, *et al.* R-SPONDIN2+ mesenchymal cells form the bud tip progenitor niche during human lung development. *Dev Cell* 2022;doi:10.1016/j.devcel.2022.05.010.
9. Lee J-H, Tammela T, Hofree M, Choi J, Marjanovic ND, Han S, *et al.* Anatomically and Functionally Distinct Lung Mesenchymal Populations Marked by Lgr5 and Lgr6. *Cell* 2017;170:1149–1163.e12.
10. Madissoon E, Oliver AJ, Kleshchevnikov V, Wilbrey-Clark A, Polanski K, Richoz N, *et al.* A spatially resolved atlas of the human lung characterizes a gland-associated immune niche. *Nat Genet* 2023;55:66–77.
11. Murthy PKL, Sontake V, Tata A, Kobayashi Y, Macadlo L, Okuda K, *et al.* Human distal lung maps and lineage hierarchies reveal a bipotent progenitor. *Nature* 2022;
12. Wang Z, Li Z, Zhou K, Wang C, Jiang L, Zhang L, *et al.* Deciphering cell lineage specification of human lung adenocarcinoma with single-cell RNA sequencing. *Nat Commun* 2021;12:6500.
13. Benahmed MA, Elbayed K, Daubeuf F, Santelmo N, Frossard N, Namer IJ. NMR HRMAS spectroscopy of lung biopsy samples: Comparison study between human, pig, rat, and mouse metabolomics. *Magn Reson Med* 2014;71:35–43.
14. Meurens F, Summerfield A, Nauwynck H, Saif L, Gerdts V. The pig: a model for human infectious diseases. *Trends Microbiol* 2012;20:50–57.
15. Lunney JK, Van Goor A, Walker KE, Hailstock T, Franklin J, Dai C. Importance of the pig as a human biomedical model. *Sci Transl Med* 2021;13:eabd5758.
16. Judge EP, Hughes JML, Egan JJ, Maguire M, Molloy EL, O'Dea S. Anatomy and bronchoscopy of the porcine lung. A model for translational respiratory medicine. *Am J Respir Cell Mol Biol* 2014;51:334–343.

17. Basil MC, Morrisey EE. Lung regeneration: a tale of mice and men. *Semin Cell Dev Biol* 2020;100:88–100.
18. Tata PR, Rajagopal J. Plasticity in the lung: making and breaking cell identity. *Development* 2017;144:755–766.
19. Polkoff KM, Gupta NK, Green AJ, Murphy Y, Chung J, Gleason KL, *et al.* LGR5 is a conserved marker of hair follicle stem cells in multiple species and is present early and throughout follicle morphogenesis. *Sci Rep* 2022;12:9104.
20. Wang Q, Liu K, Yang L, Wang H, Yang J. BoneClear: whole-tissue immunolabeling of the intact mouse bones for 3D imaging of neural anatomy and pathology. *Cell Res* 2019;29:870–872.
21. Rockich BE, Hrycaj SM, Shih HP, Nagy MS, Ferguson MAH, Kopp JL, *et al.* Sox9 plays multiple roles in the lung epithelium during branching morphogenesis. *Proc Natl Acad Sci U S A* 2013;110:E4456–64.
22. Danopoulos S, Alonso I, Thornton ME, Grubbs BH, Bellusci S, Warburton D, *et al.* Human lung branching morphogenesis is orchestrated by the spatiotemporal distribution of ACTA2, SOX2, and SOX9. *Am J Physiol Lung Cell Mol Physiol* 2018;314:L144–L149.
23. Zacharias WJ, Frank DB, Zepp JA, Morley MP, Alkhaleel FA, Kong J, *et al.* Regeneration of the lung alveolus by an evolutionarily conserved epithelial progenitor. *Nature* 2018;555:251–255.
24. Warburton D, Bellusci S, De Langhe S, Del Moral P-M, Fleury V, Mailleux A, *et al.* Molecular mechanisms of early lung specification and branching morphogenesis. *Pediatr Res* 2005;57:26R–37R.
25. Flodby P, Li C, Liu Y, Wang H, Rieger ME, Minoo P, *et al.* Cell-specific expression of aquaporin-5 (Aqp5) in alveolar epithelium is directed by GATA6/Sp1 via histone acetylation. *Sci Rep* 2017;7:3473.
26. Wang X-P, Suomalainen M, Jorgez CJ, Matzuk MM, Wankell M, Werner S, *et al.* Modulation of activin/bone morphogenetic protein signaling by follistatin is required for the morphogenesis of mouse molar teeth. *Dev Dyn* 2004;231:98–108.
27. Kongkham PN, Northcott PA, Croul SE, Smith CA, Taylor MD, Rutka JT. The SFRP family of WNT

inhibitors function as novel tumor suppressor genes epigenetically silenced in medulloblastoma. *Oncogene* 2010;29:3017–3024.

28. [No title]. at <https://academic.oup.com/bjd/article-abstract/166/5/1088/6613802>.
29. Kathiriya JJ, Wang C, Zhou M, Brumwell A, Cassandras M, Le Saux CJ, *et al.* Human alveolar type 2 epithelium transdifferentiates into metaplastic KRT5+ basal cells. *Nat Cell Biol* 2022;24:10–23.
30. McCauley KB, Hawkins F, Serra M, Thomas DC, Jacob A, Kotton DN. Efficient Derivation of Functional Human Airway Epithelium from Pluripotent Stem Cells via Temporal Regulation of Wnt Signaling. *Cell Stem Cell* 2017;20:844–857.e6.
31. Miao Q, Chen H, Luo Y, Chiu J, Chu L, Thornton ME, *et al.* Abrogation of mesenchyme-specific TGF-β signaling results in lung malformation with prenatal pulmonary cysts in mice. *Am J Physiol Lung Cell Mol Physiol* 2021;320:L1158–L1168.
32. Ahlfeld SK, Wang J, Gao Y, Snider P, Conway SJ. Initial Suppression of Transforming Growth Factor-β Signaling and Loss of TGFBI Causes Early Alveolar Structural Defects Resulting in Bronchopulmonary Dysplasia. *Am J Pathol* 2016;186:777–793.
33. Xu Z, Chen C. Abnormal Expression and Prognostic Significance of Bone Morphogenetic Proteins and Their Receptors in Lung Adenocarcinoma. *Biomed Res Int* 2021;2021:6663990.
34. Kadota T, Fujita Y, Araya J, Watanabe N, Fujimoto S, Kawamoto H, *et al.* Human bronchial epithelial cell-derived extracellular vesicle therapy for pulmonary fibrosis via inhibition of TGF-β-WNT crosstalk. *J Extracell Vesicles* 2021;10:e12124.
35. Guo X, Wang X-F. Signaling cross-talk between TGF-beta/BMP and other pathways. *Cell Res* 2009;19:71–88.
36. Subramanian A, Tamayo P, Mootha VK, Mukherjee S, Ebert BL, Gillette MA, *et al.* Gene set enrichment analysis: a knowledge-based approach for interpreting genome-wide expression profiles. *Proc Natl Acad Sci U S A* 2005;102:15545–15550.
37. Drake MG, Cook M, Fryer AD, Jacoby DB, Scott GD. Airway Sensory Nerve Plasticity in Asthma and Chronic Cough. *Front Physiol* 2021;12:720538.
38. Lauweryns JM, Van Ranst L. Protein gene product 9.5 expression in the lungs of humans and

other mammals. Immunocytochemical detection in neuroepithelial bodies, neuroendocrine cells and nerves. *Neurosci Lett* 1988;85:311–316.

39. Burns AJ, Thapar N, Barlow AJ. Development of the Neural Crest–Derived Intrinsic Innervation of the Human Lung. *Am J Respir Cell Mol Biol* 2008;38:269–275.
40. Weichselbaum M, Everett AW, Sparrow MP. Mapping the innervation of the bronchial tree in fetal and postnatal pig lung using antibodies to PGP 9.5 and SV2. *Am J Respir Cell Mol Biol* 1996;15:703–710.
41. Su Y, Barr J, Jaquish A, Xu J, Verheyden JM, Sun X. Identification of lung innervating sensory neurons and their target specificity. *Am J Physiol Lung Cell Mol Physiol* 2022;322:L50–L63.
42. Nassenstein C, Kammertoens T, Veres TZ, Uckert W, Spies E, Fuchs B, *et al.* Neuroimmune crosstalk in asthma: dual role of the neurotrophin receptor p75NTR. *J Allergy Clin Immunol* 2007;120:1089–1096.
43. Taylor-Clark TE. Molecular identity, anatomy, gene expression and function of neural crest vs. placode-derived nociceptors in the lower airways. *Neurosci Lett* 2021;742:135505.
44. Lamb JP, Sparrow MP. Three-dimensional mapping of sensory innervation with substance p in porcine bronchial mucosa: comparison with human airways. *Am J Respir Crit Care Med* 2002;166:1269–1281.
45. Kim H-S, Lee J, Lee DY, Kim Y-D, Kim JY, Lim HJ, *et al.* Schwann Cell Precursors from Human Pluripotent Stem Cells as a Potential Therapeutic Target for Myelin Repair. *Stem Cell Reports* 2017;8:1714–1726.
46. Gonzalez-Martinez T, Perez-Piñera P, Díaz-Esnal B, Vega JA. S-100 proteins in the human peripheral nervous system. *Microsc Res Tech* 2003;60:633–638.
47. Gerber D, Pereira JA, Gerber J, Tan G, Dimitrieva S, Yángüez E, *et al.* Transcriptional profiling of mouse peripheral nerves to the single-cell level to build a sciatic nerve ATlas (SNAT). *Elife* 2021;10.:
48. Toma JS, Karamboulas K, Carr MJ, Kolaj A, Yuzwa SA, Mahmud N, *et al.* Peripheral Nerve Single-Cell Analysis Identifies Mesenchymal Ligands that Promote Axonal Growth. *eNeuro*

2020;7.:

49. Wolbert J, Li X, Heming M, Mausberg AK, Akkermann D, Frydrychowicz C, *et al.* Redefining the heterogeneity of peripheral nerve cells in health and autoimmunity. *Proc Natl Acad Sci U S A* 2020;117:9466–9476.
50. Travaglini KJ, Nabhan AN, Penland L, Sinha R, Gillich A, Sit RV, *et al.* A molecular cell atlas of the human lung from single-cell RNA sequencing. *Nature* 2020;587:619–625.
51. Weber M, Apostolova G, Widera D, Mittelbronn M, Dechant G, Kaltschmidt B, *et al.* Alternative generation of CNS neural stem cells and PNS derivatives from neural crest-derived peripheral stem cells. *Stem Cells* 2015;33:574–588.
52. Chen Y-A, Lu I-L, Tsai J-W. Contactin-1/F3 Regulates Neuronal Migration and Morphogenesis Through Modulating RhoA Activity. *Frontiers in Molecular Neuroscience* 2018;
53. Zhang H, Li J, Ren J, Sun S, Ma S, Zhang W, *et al.* Single-nucleus transcriptomic landscape of primate hippocampal aging. *Protein Cell* 2021;12:695–716.
54. Sikkema L, Ramírez-Suástegui C, Strobl DC, Gillett TE, Zappia L, Madissoon E, *et al.* An integrated cell atlas of the lung in health and disease. *Nat Med* 2023;29:1563–1577.
55. Schulze H, Italiano J. *Molecular and Cellular Biology of Platelet Formation: Implications in Health and Disease*. Springer International Publishing; 2018.
56. Aros CJ, Paul MK, Pantoja CJ, Bisht B, Meneses LK, Vijayaraj P, *et al.* High-Throughput Drug Screening Identifies a Potent Wnt Inhibitor that Promotes Airway Basal Stem Cell Homeostasis. *Cell Rep* 2020;30:2055–2064.e5.
57. Aros CJ, Pantoja CJ, Gomperts BN. Wnt signaling in lung development, regeneration, and disease progression. *Commun Biol* 2021;4:601.
58. Bower DV, Lee H-K, Lansford R, Zinn K, Warburton D, Fraser SE, *et al.* Airway branching has conserved needs for local parasympathetic innervation but not neurotransmission. *BMC Biol* 2014;12:92.
59. Knox SM, Lombaert IMA, Haddox CL, Abrams SR, Cotrim A, Wilson AJ, *et al.* Parasympathetic stimulation improves epithelial organ regeneration. *Nat Commun* 2013;4:1494.

60. Audrit KJ, Delventhal L, Aydin Ö, Nassenstein C. The nervous system of airways and its remodeling in inflammatory lung diseases. *Cell Tissue Res* 2017;367:571–590.

61. Kaelberer MM, Caceres AI, Jordt S-E. Activation of a nerve injury transcriptional signature in airway-innervating sensory neurons after lipopolysaccharide-induced lung inflammation. *Am J Physiol Lung Cell Mol Physiol* 2020;318:L953–L964.

62. Koopmans T, Gosens R. Revisiting asthma therapeutics: focus on WNT signal transduction. *Drug Discov Today* 2018;23:49–62.

63. Hachim MY, Elemam NM, Ramakrishnan RK, Bajbouj K, Olivenstein R, Hachim IY, *et al.* Wnt Signaling Is Deranged in Asthmatic Bronchial Epithelium and Fibroblasts. *Front Cell Dev Biol* 2021;9:641404.

64. Singla A, Reuter S, Taube C, Peters M, Peters K. The molecular mechanisms of remodeling in asthma, COPD and IPF with a special emphasis on the complex role of Wnt5A. *Inflamm Res* 2023;72:577–588.

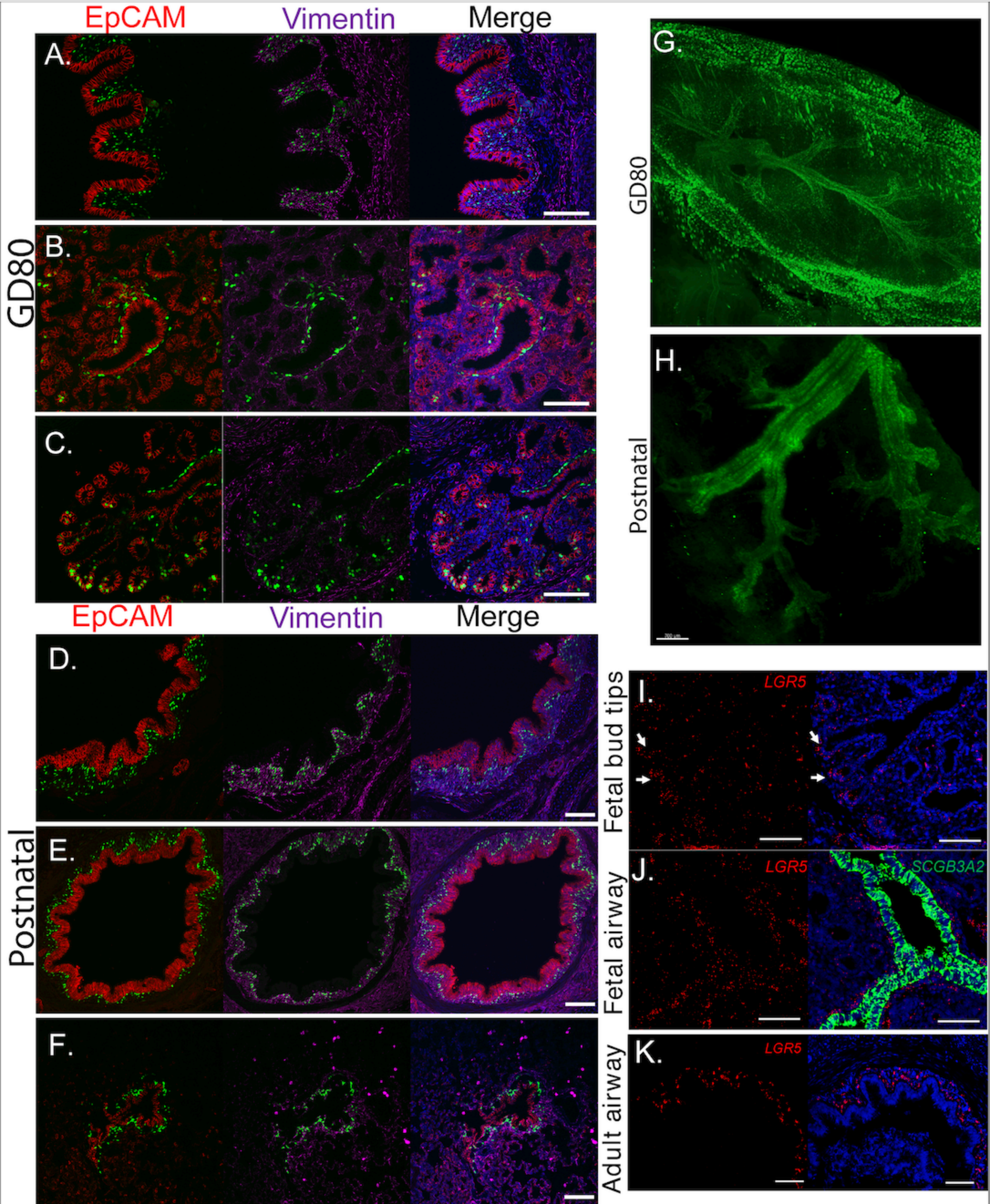
EpCAM
Vimentin
Merge
A.
B.
C.
GD80
EpCAM
Vimentin
Merge
D.
E.
F.
Postnatal
G.
GD80
H.
Postnatal
I.
LGR5
Fetal bud tips
J.
LGR5
SCGB3A2
Fetal airway
K.
LGR5
Adult airway

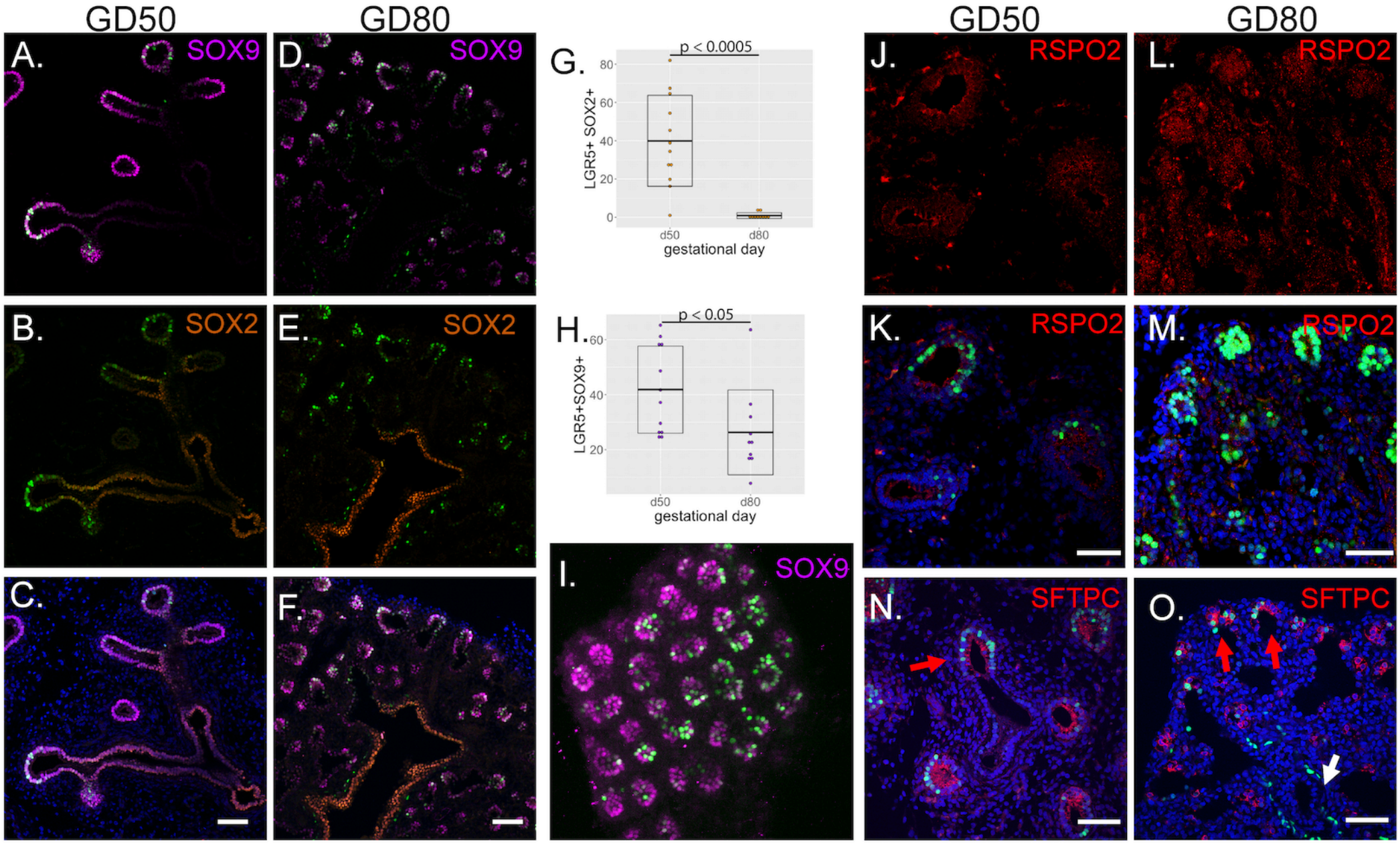
GD50
GD80
A.
SOX9
D.
SOX9
B.
SOX2
E.
SOX2
C.
F.
G.
p < 0.0005
LGR5+ SOX2+
80
60
40
20
0
d50
d80
gestational day
H.
p < 0.05
LGR5+SOX9+
60
40
20
d50
d80
gestational day
I.
SOX9
GD50
GD80
J.
RSPO2
L.
RSPO2
K.
RSPO2
M.
RSPO2
N.
SFTPC
O.
SFTPC

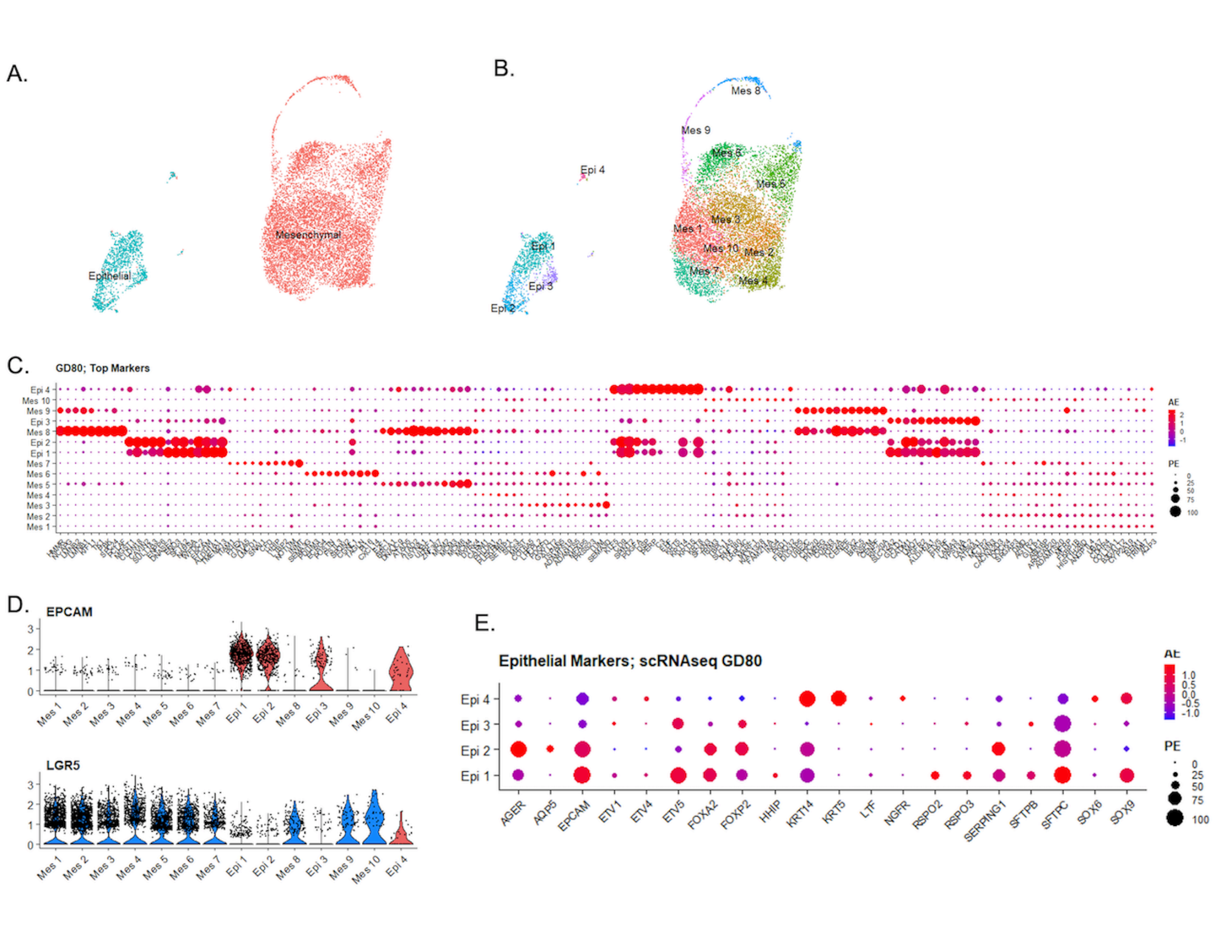
A.
Mesenchymal
Epithelial
B.
Mes 8
Mes 9
Mes 6
Epi 4
Mes 5
Mes 3
Mes 1
Mes 10
Mes 2
Mes 7
Mes 4
Epi 1
Epi 3
Epi 2
C.
GD80; Top Markers
Epi 4
Mes 10
Mes 9
Epi 3
Mes 8
Epi 2
Epi 1
Mes 7
Mes 6
Mes 5
Mes 4
Mes 3
Mes 2
Mes 1
AE
PE
D.
EPCAM
LGR5
Mes 1
Mes 2
Mes 3
Mes 4
Mes 5
Mes 6
Mes 7
Epi 1
Epi 2
Mes 8
Epi 3
Mes 9
Mes 10
Epi 4
E.
Epithelial Markers; scRNAseq GD80
Epi 4
Epi 3
Epi 2
Epi 1
AGER
AQP5
EPCAM
ETV1
ETV4
ETV5
FOXA2
FOXP2
HHIP
KRT14
KRT5
LTF
NGFR
RSPO2
RSPO3
SERPING1
SFTPB
SFTPC
SOX6
SOX9
AE
PE

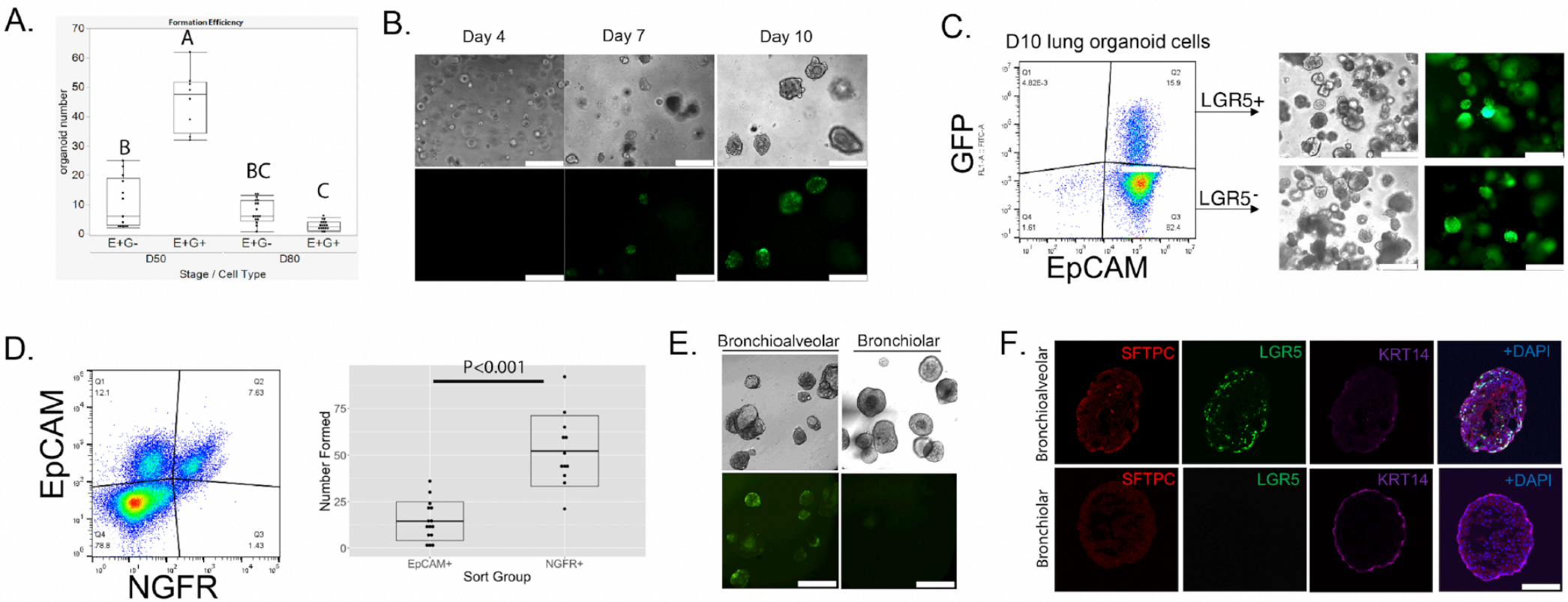
A.
Formation Efficiency
organoid number
70
60
50
40
30
20
10
0
A
B
BC
C
E+G-
E+G+
E+G-
E+G+
D50
D80
Stage / Cell Type
B.
Day 4
Day 7
Day 10
C.
D10 lung organoid cells
GFP
EpCAM
LGR5+
LGR5-
D.
EpCAM
NGFR
Q1
12.1
Q2
7.63
Q4
78.8
Q3
1.43
P<0.001
Number Formed
75
50
25
0
EpCAM+
NGFR+
Sort Group
E.
Bronchioalveolar
Bronchiolar
F.
Bronchioalveolar
Bronchiolar
SFTPC
LGR5
KRT14
+DAPI

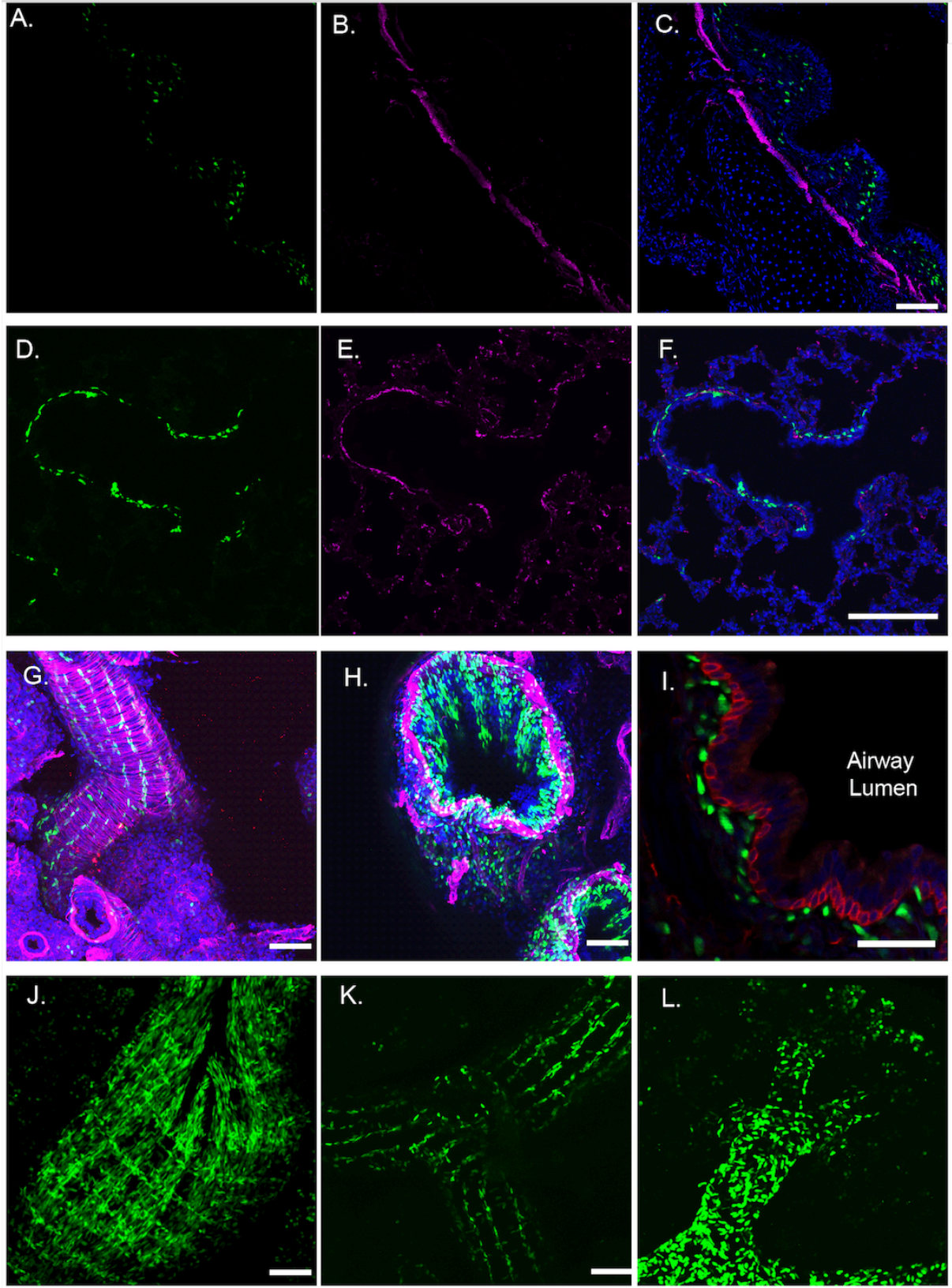
A.
B.
C.
D.
E.
F.
G.
H.
I.
Airway
Lumen
J.
K.
L.

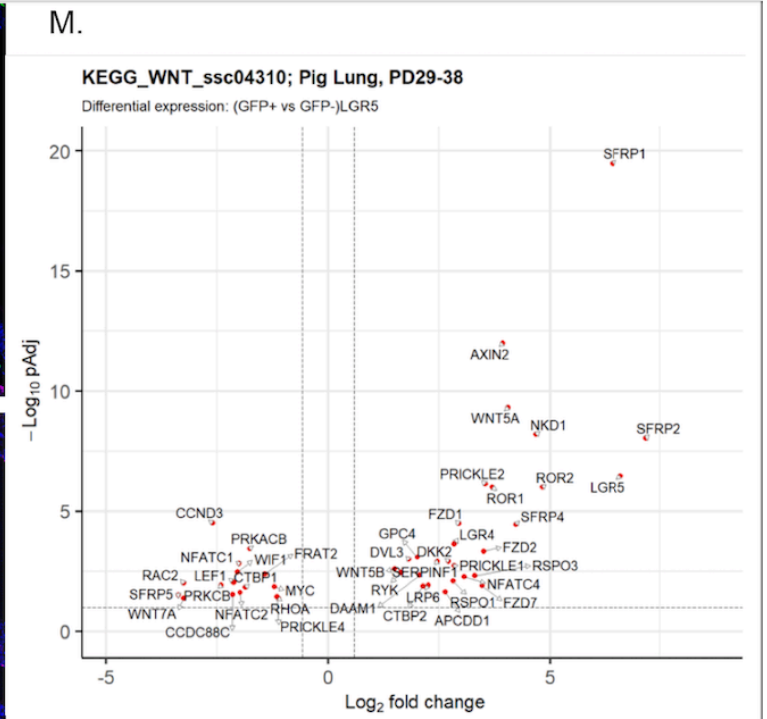
M.
KEGG_WNT_ssc04310; Pig Lung, PD29-38
Differential expression: (GFP+ vs GFP-)LGR5
−Log10 pAdj
Log2 fold change
SFRP1
AXIN2
WNT5A
NKD1
SFRP2
PRICKLE2
ROR2
LGR5
ROR1
CCND3
FZD1
SFRP4
PRKACB
GPC4
LGR4
NFATC1
WIF1
FRAT2
DVL3
DKK2
FZD2
RAC2
LEF1
CTBP1
WNT5B
SERPINF1
PRICKLE1
RSPO3
SFRP5
PRKCB
MYC
RYK
NFATC4
LRP6
RSPO1
FZD7
WNT7A
NFATC2
RHOA
DAAM1
CTBP2
APCDD1
CCDC88C
PRICKLE4

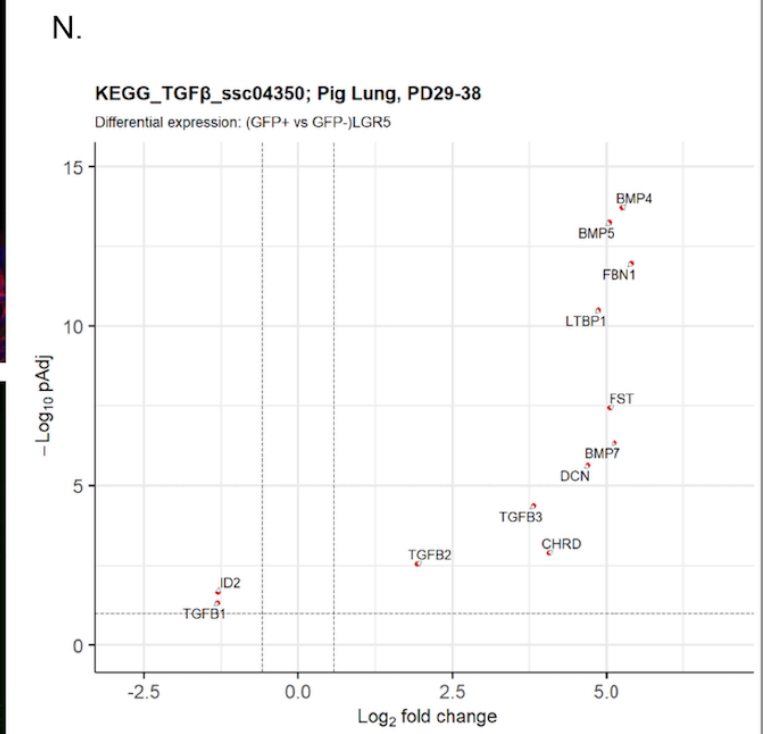
N.
KEGG_TGFβ_ssc04350; Pig Lung, PD29-38
Differential expression: (GFP+ vs GFP-)LGR5
−Log10 pAdj
Log2 fold change
BMP4
BMP5
FBN1
LTBP1
FST
BMP7
DCN
TGFB3
CHRD
TGFB2
ID2
TGFB1

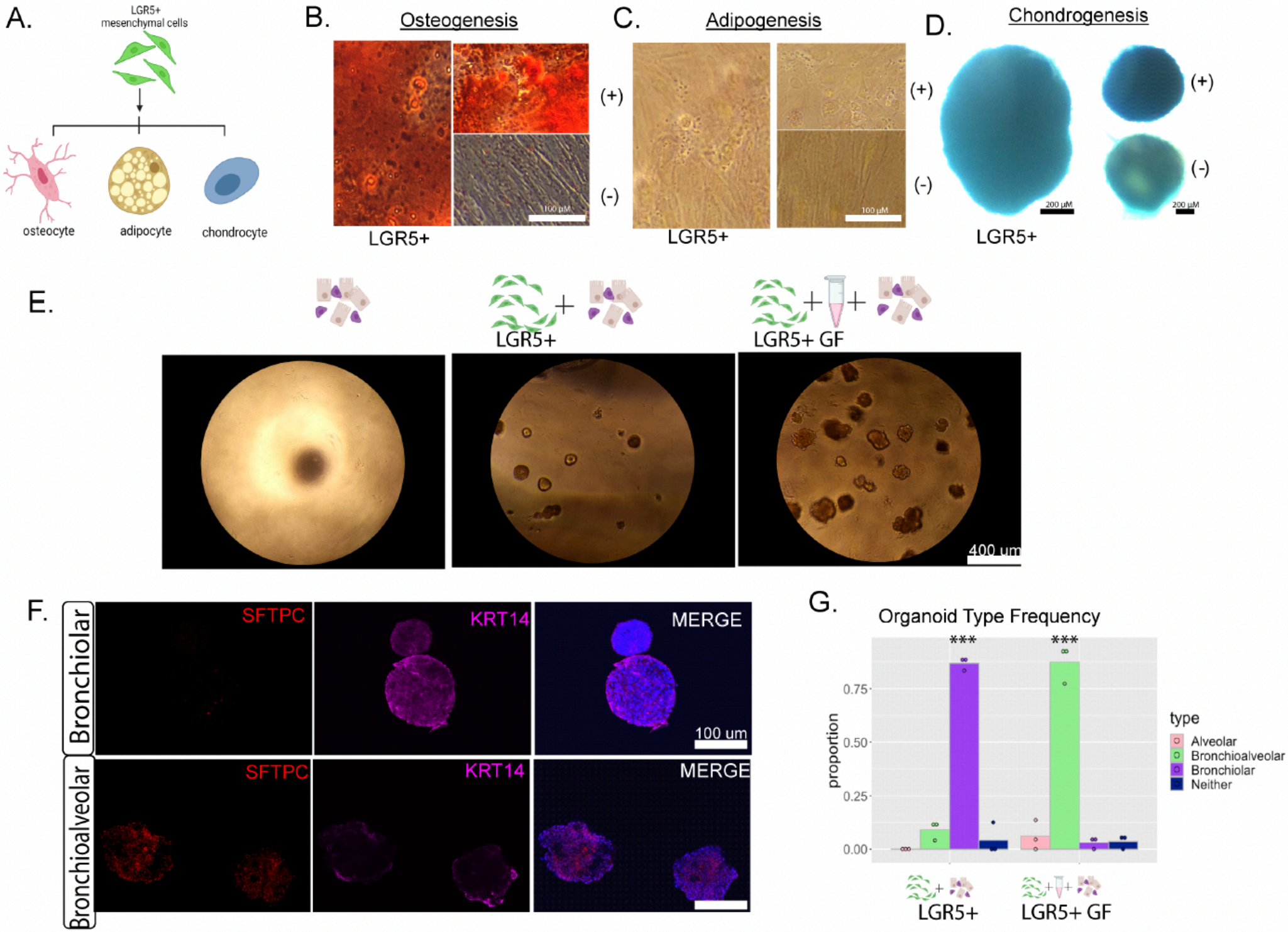
A.
LGR5+ mesenchymal cells
osteocyte
adipocyte
chondrocyte
B.
Osteogenesis
(+)
(-)
100 µM
LGR5+
C.
Adipogenesis
(+)
(-)
100 µM
LGR5+
D.
Chondrogenesis
(+)
(-)
200 µM
200 µM
LGR5+
E.
LGR5+
LGR5+ GF
400 um
F.
Bronchiolar
Bronchioalveolar
SFTPC
KRT14
MERGE
100 um
G.
Organoid Type Frequency
***
***
proportion
0.75
0.50
0.25
0.00
type
Alveolar
Bronchioalveolar
Bronchiolar
Neither
LGR5+
LGR5+ GF

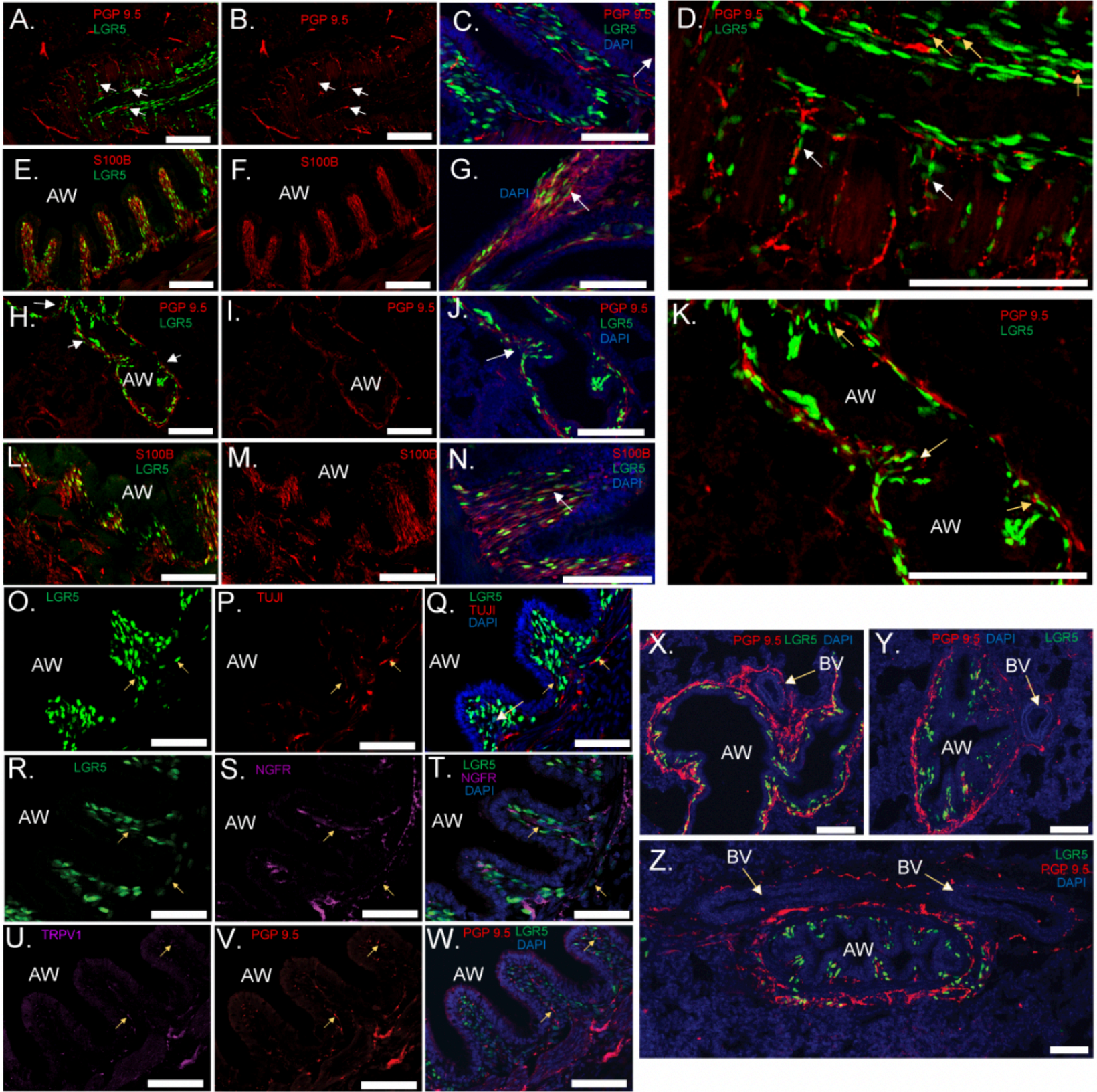
A.
PGP 9.5
LGR5
B.
PGP 9.5
C.
PGP 9.5
LGR5
DAPI
D.
PGP 9.5
LGR5
E.
S100B
LGR5
AW
F.
S100B
AW
G.
DAPI
H.
PGP 9.5
LGR5
AW
I.
PGP 9.5
AW
J.
PGP 9.5
LGR5
DAPI
K.
PGP 9.5
LGR5
AW
AW
L.
S100B
LGR5
AW
M.
AW
S100B
N.
S100B
LGR5
DAPI
O.
LGR5
AW
P.
TUJI
AW
Q.
LGR5
TUJI
DAPI
AW
R.
LGR5
AW
S.
NGFR
AW
T.
LGR5
NGFR
DAPI
AW
U.
TRPV1
AW
V.
PGP 9.5
AW
W.
PGP 9.5
LGR5
DAPI
AW
X.
PGP 9.5 LGR5 DAPI
BV
AW
Y.
PGP 9.5 DAPI
LGR5
BV
AW
Z.
BV
BV
LGR5
PGP 9.5
DAPI
AW